

Dynamics of Wing Cracks and Nanoscale Damage in Glass

Zhen Lu, Ken-ichi Nomura, Ashish Sharma, Weiqiang Wang, Cheng Zhang, Aiichiro Nakano,
Rajiv Kalia,* and Priya Vashishta

*Collaboratory for Advanced Computing and Simulations, University of Southern California,
Los Angeles, California 90089-0242, USA*

Elisabeth Bouchaud and Cindy Rountree

Service de Physique et de Chimie des Surfaces et Interfaces, CEA-Saclay, DSM/DRECAM/SPCSI 91191 Gif Sur Yvette Cedex, France
(Received 19 March 2005; published 20 September 2005)

We investigate initiation, growth, and healing of wing cracks in confined silica glass by molecular dynamics simulations. Under dynamic compression, frictional sliding of precrack surfaces nucleates nanovoids which evolve into nanocrack columns at the precrack tip. Nanocrack columns merge to form a wing crack, which grows via coalescence with nanovoids in the direction of maximum compression. Lateral confinement arrests the growth and partially heals the wing crack. Growth and arrest of the wing crack occur repeatedly, as observed in dynamic compression experiments on brittle solids under lateral confinement.

DOI: [10.1103/PhysRevLett.95.135501](https://doi.org/10.1103/PhysRevLett.95.135501)

PACS numbers: 62.20.Mk, 31.15.Qg, 62.30.+d

Crack initiation and growth in brittle solids under *tension* have been extensively studied by various experimental, theoretical, and numerical simulation approaches [1]. In contrast, relatively little work has been done in the area of compressive fracture despite its vital importance in geology and materials science and engineering applications. Experiments and continuum models have been used to investigate the influence of compressive stresses on cracks embedded in brittle solids [2–10]. These studies reveal that the surfaces of a crack slide under multiaxial compression when the resolved applied shear stress exceeds frictional stress due to normal forces on the crack surfaces. The sliding motion generates tensile stresses at the crack tip where wing cracks are formed. Wing cracks have been observed in glasses [3], ceramics [4,5], and various rocks [7]; and satellite images have revealed tens of kilometer long wing cracks in arctic ice [8]. Macroscopic observations [4,5,7] and continuum models [9–11] show that wing cracks initiate at an angle of 70.5° relative to the precrack and then turn in the direction of maximum compression. Their growth is limited by pressure due to lateral confinement. Experimental and theoretical efforts have not been able to ascertain damage mechanisms underlying initiation, growth, and arrest of wing cracks at the level of material heterogeneities.

In this Letter, we present molecular dynamics (MD) simulation results that reveal atomistic mechanisms of wing-crack initiation, growth, arrest, and healing in a confined, precracked silica glass. Under the influence of dynamic compression, crack surfaces slide upon the arrival of a compression wave and the precrack tip kinks towards a tensile region containing nanometer scale cavities. The kink angle is in agreement with macroscopic observations on various brittle materials [4,7,9,11]. MD simulations

further reveal that damage nanocavities around the precrack coalesce with kinks to form crack nanocolumns which develop into a wing crack. Coalescence with nanocavities accelerates segments of the wing-crack tip to supersonic speeds, although the average wing-crack speed ranges between 30–50% of the speed of Rayleigh waves. The wing crack grows along the direction of maximum compression. Interaction with a compression wave reflected from the lateral side of the simulation cell partially heals the wing crack and nanocavities, but they grow again after the passage of the compression wave. In dynamic compression experiments on brittle materials, Lee and Ravichandran have observed repeated “initiation, growth, and arrest” of a wing crack due to wave reflection from specimen edges [4].

MD simulations reported here are based on a combination of two- and three-body interatomic potentials [12] which were validated by measurements of structural correlations [13], elastic moduli [14], fracture toughness [15,16], and phonon density of states [13]. We first prepared a 15×10^6 -atom amorphous system by melting an ideal β -cristobalite crystal and quenching the molten state in a box of dimensions $1200 \times 1200 \times 150 \text{ \AA}$ with periodic boundary conditions [12]. Subsequently, periodic boundary conditions were removed and a precrack of length 400 \AA was inserted. Figure 1(a) schematically shows the amorphous system (blue) with the precrack and a rigid indenter (gray) that moves at a constant velocity in the x direction and exerts a repulsive force on atoms above the precrack surface. The indenter speeds, v_{impact} , were chosen to be 5% and 12.5% of the Rayleigh wave speed in silica glass ($v_R \approx 3000 \text{ m/s}$). Lateral confinement was imposed by having walls around the system. Atoms interacted with the walls via a short-ranged repulsive potential. To study

the effect of compression-wave reflection from boundaries, simulations were performed without and with damping on atoms near the boundaries [17].

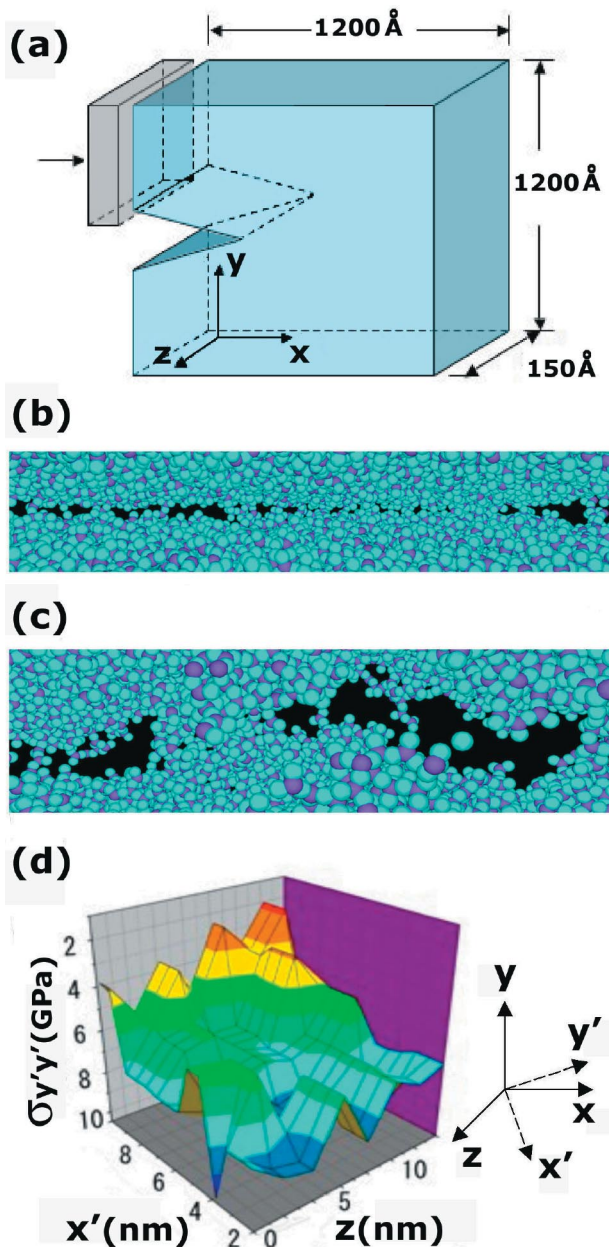


FIG. 1 (color). (a) In the MD simulation setup, the gray rectangular plate is a rigid indenter and the blue parallelepiped represents silica glass with a precrack; (b) snapshot of the precrack tip with atoms and nanocavities (black) due to frictional sliding of the crack surfaces; (c) atomistic view of kinks formed by nanocavities (black); (d) tensile stress $\sigma_{y'y'}$ along the crack front (z) as a function of the distance, x' , from the precrack tip in the primed coordinate system which is rotated 70° around the z axis. Only a part of the simulation cell is shown in (b), (c), and (d). The impact speed is $\nu_{\text{impact}} = 0.05\nu_R$, where ν_R is the Rayleigh wave speed.

For each atomic configuration, the morphology and dynamics of cracks and damage cavities were analyzed by dividing the simulation box into voxels (three-dimensional cubic cells of size 4.5 \AA , which is the second nearest neighbor Si-O distance) and by using the linked-list method to determine voxels without atoms [16,18,19]. Empty voxels were assigned IDs such that those with the same ID either corresponded to a distinct pore or were linked to the crack. Pore and crack boundaries were determined from the positions of atoms closest to the outermost empty voxels.

We calculated stresses around the precrack tip immediately after the load was applied. For distances greater than 100 \AA from the tip, the radial and angular dependences of atomistic-level stresses are in good agreement with mode II stress distributions in linear elastic fracture mechanics (LEFM) [1]. However, for distances less than 100 \AA from the precrack tip, the discrete nature of the material becomes relevant and the stresses in the MD simulation differ significantly from LEFM results.

Yet, surprisingly, the MD results are in agreement with LEFM for the direction in which the precrack kinks. As the indenter moves, a compression wave is generated which propagates from left to right in Fig. 1(a) [20]. The top and bottom surfaces of the precrack begin to slide and, as shown in Fig. 1(b), nanometer scale cavities (black) appear at the tip after the arrival of the compression wave. These cavities grow and kink towards a tensile region near the precrack tip. Figure 1(c) is a snapshot of the spatial distribution of these nanocavities (black) and Fig. 1(d) shows the stress component $\sigma_{y'y'}$ perpendicular to the direction in which nanocavities nucleate. (The precrack kinks towards x' .) The stress is tensile up to $x' = 100 \text{ \AA}$ from the precrack tip. The crack tip bends 70° towards maximum mode I tension, as predicted theoretically [11] and observed macroscopically in quasistatic and dynamic compression experiments on brittle materials [4,5,7].

In MD simulations, we observe that nanocavities coalesce with kinks to form crack nanocolumns. Figure 2 (top) is a snapshot of nanocrack columns (gray voxels) hanging from the precrack and nanocavities (red, orange, yellow and green voxels) in the tensile region. Figure 2 (middle) shows the growth of nanocrack columns and formation of new voids around them. In Fig. 2 (bottom), nanocrack columns have merged to form a wing crack, which propagates at an average velocity of $1,000 \text{ m/s}$. Spatial fluctuations in the velocity along the wing-crack front [along z ; see Fig. 1(a)] can be significant, especially when segments of the wing-crack tip coalesce with cavities and accelerate to supersonic speeds. Damage nanocavities continue to nucleate in the tensile region ahead of the moving crack front and the maximum range of the damage zone is about 300 \AA . After reaching a length of 90 \AA , the growth of the wing crack ceases and in the next 7 ps the wing crack heals at an average speed of $1,300 \text{ m/s}$.

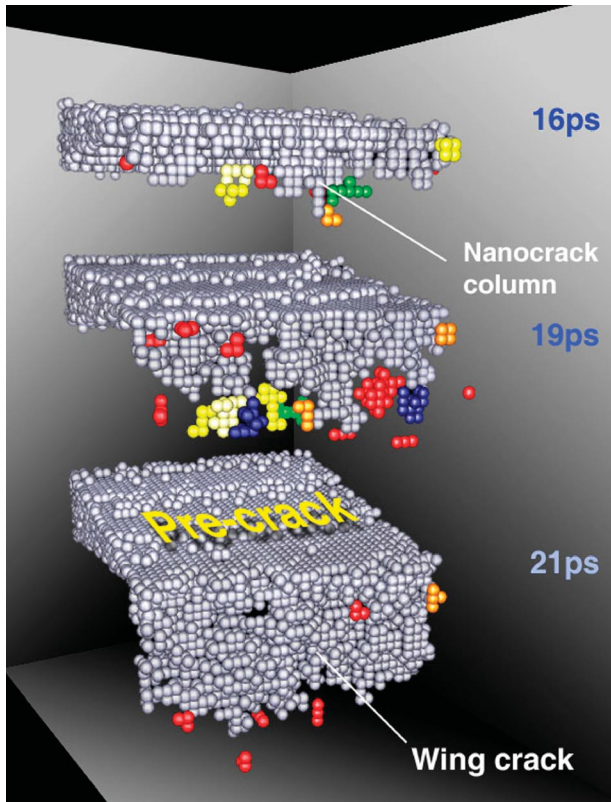


FIG. 2 (color). Wing-crack formation at $\nu_{\text{impact}} = 0.05\nu_R$. Only a part of the simulation cell and the precrack are shown. Spheres are voxels and different colors show different nanocavities. (Top) Nanocrack columns (gray) and damage nanocavities (color) in the tensile stress region of Fig. 1(d); (Middle) snapshot shows the growth of nanocrack columns and formation of new cavities; and (Bottom) nanocrack columns grow and coalesce with nanocavities to form a wing crack.

While the wing crack is healing, the primary crack begins to advance in the direction of impact loading. Nanoscale damage cavities continue to form and coalesce with the moving primary crack and the crack length increases by 50 Å over 11 ps. Subsequently, the primary crack stops and is partially healed while the wing crack reemerges and propagates at an average speed of 1,500 m/s. Figure 3 displays three events during the second retreat of the wing crack after it reaches a maximum length of 270 Å. The right snapshot, taken just after the wing crack encounters the compression wave due to lateral confinement, shows two large damage cavities (green and red) at the wing-crack tip and a few cavities ahead of the primary crack. The middle snapshot (76 ps) shows two large (blue and green) and a few small nanocavities (red and yellow) left behind by the receding wing crack and the left snapshot shows the wing crack and damage cavities after the second healing stops (80 ps). The average speed of the receding wing crack is about 800 m/s and the residual length of the wing crack is 130 Å. On running the simula-

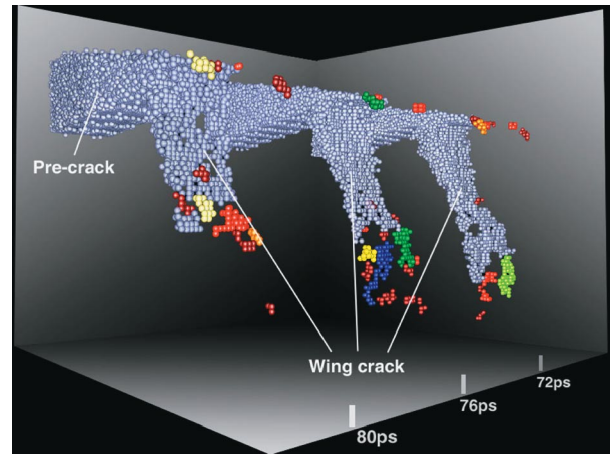


FIG. 3 (color). Second healing of the wing crack at $\nu_{\text{impact}} = 0.05\nu_R$. Right: Snapshot of the wing and primary cracks just after the wing-crack growth is arrested. The wing-crack tip is split into two columns and there are a few damage cavities (green and red) near the tip. Middle: In the next 4 ps the wing crack recedes considerably and leaves behind damage cavities (red, yellow, green, and blue). Left: Snapshot of the wing crack and cavities after the healing stops.

tion longer, we find that the wing crack propagates and retreats repeatedly. Repeated initiation, growth, and arrest of wing cracks have also been observed in dynamic compression experiments on ceramic glass under lateral confinement [4].

At the higher impact loading speed, $\nu_{\text{impact}} = 0.125\nu_R$, the precrack tip again kinks towards maximum mode I tension (70° around the z axis) and nanocavities and nanocrack columns coalesce to form a wing crack. The wing crack grows to a length of 210 Å over 17.5 ps and then propagates in the direction of maximum compression at one-third the speed of Rayleigh waves for about 10 ps. Quasistatic and dynamic compression experiments also reveal that wing cracks always turn in the direction of maximum compression [4].

The subsequent retreat of the wing crack is quite different from that at the lower impact loading speed. In Fig. 4, the snapshot taken at 40 ps shows the wing crack and nanocavities just after the crack reaches a maximum length of 310 Å. The middle snapshot shows an encounter between the wing crack and compression wave reflected from the sidewalls, which splits off a 200 Å long cavity (red). Shortly after the passage of the compression wave, the crack and the cavity rejoin and continue to heal. The left snapshot shows a secondary wing crack behind and residual damage cavities ahead of the retreating crack. This growth-and-retreat sequence of the wing crack is observed repeatedly.

In conclusion, MD simulations reveal that frictional sliding of precrack surfaces in silica glass under dynamic compression initiates damage in the form of nanocavitation, which is intrinsically linked to the amorphous struc-

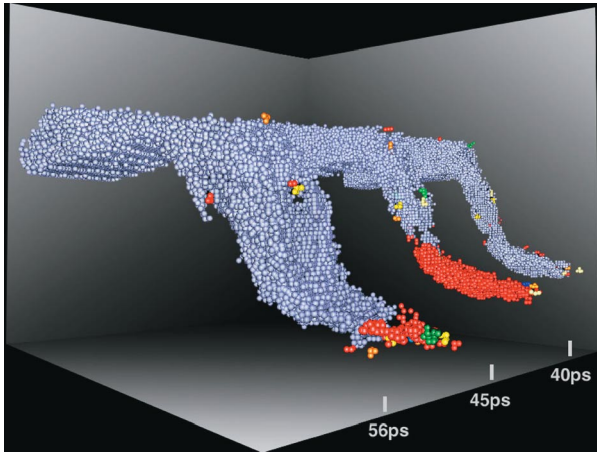


FIG. 4 (color). Snapshots of the wing crack and nanocavities at $v_{\text{impact}} = 0.125v_R$. Right: snapshot shows the wing crack turned in the direction of the applied load; Middle: a large cavity (red) splits off the wing crack; Left: after 4 ps the wing crack and the cavity rejoin and the crack recedes by 6 nm. A secondary wing crack appears behind the main wing crack.

ture and is the main growth mechanism for the wing crack. The wing crack and nanocavities heal partially under the influence of the compression wave reflected from the sides of the confined sample. We have also performed simulations with Langevin dynamics [17] on atoms in boundary layers to suppress reflection of compression waves. Results for the wing-crack initiation and growth remain unchanged. The wing crack is still arrested by confinement, but the damage due to cavities left behind by healing is more extensive than in the absence of damping. Thus, when the wing crack reemerges, it propagates more rapidly via coalescence with cavities in the damage zone. The growth and coalescence of nanocavities with an advancing crack have also been observed in recent atomic force microscope (AFM) experiments on stress corrosion cracking of glasses [21], while repeated initiation, growth, and arrest of wing cracks have been reported in dynamic compression experiments on ceramic glass under lateral confinement [4].

This research was supported by Grants from ARO, DARPA, DOE, NSF, and a DoD Challenge project. We thank Dr. Daniel Bonamy for fruitful discussions.

*Email address: rkalia@usc.edu

- [1] T.L. Anderson, *Fracture Mechanics* (CRC Press, New York, 1995), 2nd ed..
- [2] S. Nemat-Nasser and H. Horii, *J. Geophys. Res.* **87**, 6805 (1982); H. Horii and S. Nemat-Nasser, *J. Geophys. Res.* **90**, 3105 (1985).
- [3] W.F. Brace and E. G. Bombolakis, *J. Geophys. Res.* **68**, 3709 (1963).
- [4] S. Lee and G. Ravichandran, *Optics and Lasers in Engineering* **40**, 341 (2003); *Eng. Fract. Mech.* **70**, 1645 (2003).
- [5] W.N. Chen and G. Ravichandran, *J. Mech. Phys. Solids* **45**, 1303 (1997).
- [6] R. Carl-Ernst and A.J. Rosakis, *J. Geophys. Res.* **108**, 2411 (2003).
- [7] M.F. Ashby and S.D. Hallam, *Acta Metall.* **34**, 497 (1986); M.F. Ashby and C.G. Sammis, *Pure Appl. Geophys.* **133**, 489 (1990).
- [8] E.M. Schulson, *JOM* **51**, 21 (1999); C.E. Renshaw and M. Schulson, *Nature (London)* **412**, 897 (2001).
- [9] F. Lehner and M. Kachanov, *Int. J. Fract.* **77**, R69 (1996).
- [10] G. Ravichandran and G. Subhash, *Int. J. Solids Struct.* **32**, 2627 (1995).
- [11] B. Cotterell and J.R. Rice, *Int. J. Fract.* **16**, 155 (1980).
- [12] P. Vashishta, R. K. Kalia, J.P. Rino, and I. Ebbsjö, *Phys. Rev. B* **41**, 12197 (1990); P. Vashishta, R. K. Kalia, A. Nakano, W. Li, and I. Ebbsjö, in *Amorphous Insulators and Semiconductors*, edited by M.F. Thorpe and M.I. Mitkova (Kluwer, Dordrecht, 1996), p. 151.
- [13] D.L. Price, *Curr. Opin. Solid State Mater. Sci.* **1**, 572 (1996).
- [14] Q. Wang *et al.*, *J. Non-Cryst. Solids* **143**, 65 (1992).
- [15] J.P. Lucas *et al.*, *Scr. Metall. Mater.* **32**, 743 (1995).
- [16] C.L. Rountree, Ph.D. thesis, Louisiana State University.
- [17] To suppress compression-wave reflection from the cell boundaries, atoms within 100 Å from a wall were treated by Langevin dynamics with a continuously increasing damping constant; see M.P. Allen and D.J. Tildesley, *Computer Simulation of Liquids* (Oxford University Press, Oxford, 1987).
- [18] M. Buehler, F. Abraham, and H. Gao, *Nature (London)* **426**, 141 (2003).
- [19] K. S. Cheung and S. Yip, *Phys. Rev. Lett.* **65**, 2804 (1990).
- [20] Static structure factor and Si-O-Si bond angle distribution indicate plasticity in the compressed region. However, compression is much less than that for structural transformation; see R.M. Wentzcovitch, C. de Silva, J.R. Chelikowsky, and N. Binggli, *Phys. Rev. Lett.* **80**, 2149 (1998).
- [21] F. Célarié *et al.*, *Phys. Rev. Lett.* **90**, 075504 (2003). These AFM experiments contradict the commonly held belief that cracks propagate through glass without causing any damage; See J.P. Guin and S. M. Wiederhorn, *Phys. Rev. Lett.* **92**, 215502 (2004).